Ultrasmall Antioxidant Cerium Oxide Nanoparticles for Regulation of Acute Inflammation

Johoon Kim,

Department of Radiology and Department of Bioengineering, University of Pennsylvania, Philadelphia, Pennsylvania 19104, United States;

Gwanui Hong,

Institute for Translational Medicine and Therapeutics, University of Pennsylvania, Philadelphia, Pennsylvania 19104, United States

Luda Mazaleuskaya,

Institute for Translational Medicine and Therapeutics, University of Pennsylvania, Philadelphia, Pennsylvania 19104, United States

Jessica C. Hsu,

Department of Radiology and Department of Bioengineering, University of Pennsylvania, Philadelphia, Pennsylvania 19104, United States;

Derick N. Rosario-Berrios,

Department of Biochemistry and Molecular Biophysics, University of Pennsylvania, Philadelphia, Pennsylvania 19104, United States

Tilo Grosser,

Institute for Translational Medicine and Therapeutics, University of Pennsylvania, Philadelphia, Pennsylvania 19104, United States

Park F. Cho-Park,

Institute for Translational Medicine and Therapeutics, University of Pennsylvania, Philadelphia, Pennsylvania 19104, United States

David P. Cormode

Corresponding Author: **David P. Cormode** – Department of Radiology, Department of Bioengineering, and Department of Biochemistry and Molecular Biophysics, University of Pennsylvania, Philadelphia, Pennsylvania 19104, United States; Phone: 215-615-4656; David.Cormode@pennmedicine.upenn.edu; Fax: 240-368-8096.

Complete contact information is available at: https://pubs.acs.org/10.1021/acsami.1c16126

Department of Radiology, Department of Bioengineering, and Department of Biochemistry and Molecular Biophysics, University of Pennsylvania, Philadelphia, Pennsylvania 19104, United States;

Abstract

Cerium oxide nanoparticles (CeONP), having potent antioxidant properties, are highly promising nanomaterials for treatment of diseases in which oxidative stress from excessive reactive oxygen species (ROS) plays a critical role in the pathogenesis and progression. However, most previously reported CeONP formulations were not efficiently cleared from the body, precluding their clinical translation. Herein, we report ultrasmall CeONP that can mitigate activation of macrophages and subsequent acute inflammation. It is found that these CeONP can effectively scavenge reactive species, inhibit macrophage activation, and minimize their recruitment and infiltration to the inflammation site, which lead to alleviation of edema and pain hypersensitivity. Moreover, we demonstrate that CeONP can be effectively excreted from the body within 24 h of systemic administration, minimizing long-term toxicity concerns. Altogether, our findings suggest that CeONP may be explored as both antioxidant and anti-inflammatory agents that can reduce acute inflammation with a better safety profile than existing nanoparticles.

Graphical Abstract
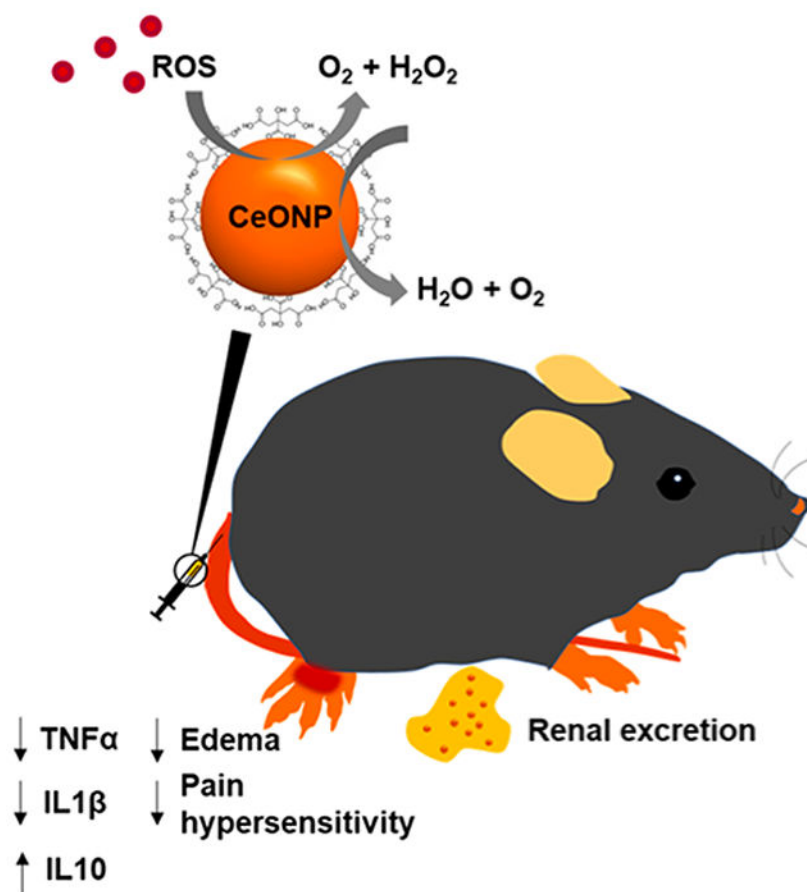
1. INTRODUCTION

Reactive oxygen species (ROS) are natural byproducts of oxygen metabolism that is essential for cell signaling; however, production of excess ROS can have detrimental effects on cells, causing oxidative damage to various cellular components, such as DNA, proteins, and lipids, and subsequent cell death and tissue damage.[1] Elevated production of free radicals from the imbalance between their production and elimination by endogenous catalytic mechanisms is defined as oxidative stress.[2,3] Oxidative stress is a key contributor in progression of inflammatory diseases as well as acute injury and inflammation.[4] Oxidative stress promotes inflammation by directly activating the expression of proinflammatory genes and inhibit tissue remodeling.[5] These initial Inflammatory processes can cause healthy tissue injury and exacerbate ROS production from phagocytic cells, such as macrophages and neutrophils.[4,6] Therefore, restoration of ROS homeostasis via delivery of antioxidant agent is a promising therapeutic approach to prevent collateral healthy tissue damage from oxidative stress and inflammation.

Emerging nanomaterials that can offer novel treatment options for oxidative stress-related diseases are nanozymes.[7] Nanozymes are capable of mimicking the catalytic activities of natural enzymes to efficiently scavenge ROS in their surroundings. A class of nanozymes called CeONP have attracted substantial research interest.[8–13] Cerium ions in CeONP can exist in one of two oxidation states (Ce^{3+} and Ce^{4+}) on the nanoparticle surface, and highly mobile oxygen vacancies in the lattice allow these cerium ions to freely alternate their oxidation states in a reversible manner.[14–16] Through this interchange in redox state, each reactive site on CeONP can interact with numerous ROS molecules and convert them to inert molecules, allowing CeONP to have more potent antioxidative activities than traditional antioxidants (e.g., vitamin C and selenium). In addition, the presence of multiple reactive sites on the nanoparticles surfaces further augments the antioxidant properties of CeONP to allow sustained catalytic activity.

CeONP's strong catalytic activity through the redox reaction has already been well-recognized and widely applied in petrochemical and materials industry.[17–19] More recently, CeONP have been increasingly investigated for the treatment of ROS-related diseases, including neurodegenerative diseases,[20,21] autoimmune diseases,[22] ocular surface diseases,[13] and ischemic and acute injuries.[23–27] Potential biomedical applications of CeONP are favorable since their ROS scavenging mechanism is analogous to biological processes that are used by endogenous enzymes in our body, such as superoxide dismutase (SOD) and catalase.[28–30] By designing our CeONP formulation to be ultrasmall, we further improved its feasibility in biomedical uses. Small hydrodynamic sizes of CeONP improve the chance of eventual clinical translation by promoting efficient renal clearance and thereby addresses toxicity concerns that arise from long-term retention in the reticuloendothelial system.[31,32]

Herein, we demonstrate that citric acid-coated CeONP with strong antioxidant properties can alleviate inflammation-induced edema and pain hypersensitivity by reducing secretion of proinflammatory cytokines and suppressing macrophage recruitment to the inflammation site. Moreover, we investigate the toxicity and renal clearance of the CeONP formulation, which are key parameters to be considered for eventual clinical translation.

2. MATERIALS AND METHODS

2.1. Materials.

Cerium(III) nitrate hexahydrate (99.99%) and ammonium hydroxide (28.0–30.0% NH_3 basis) were obtained from Sigma-Aldrich. Citric acid (anhydrous), the superoxide dismutase colorimetric activity kit, the Amplex red hydrogen peroxide/peroxidase assay kit, 2′,7′-dichlorodihydrofluorescein diacetate (CM-H2DCFDA), and mouse TNF alpha and IL-1β ELISA kits were purchased from Thermofisher Scientific. The hydroxyl radical antioxidant capacity (HORAC) activity assay was purchased from Cell Biolabs. The mouse IL-10 ELISA kit was acquired from Abcam. HepG2, RAW 264.7, Renca, and SVEC4-10EHR1 cell lines were purchased from ATCC.

2.2. Synthesis of Citric Acid-Coated CeONP.

Ultrasmall citric acid-coated CeONP were synthesized by slight modification of an alkaline-based precipitation method that our group has previously reported.[33] Briefly, a 4 mL solution containing 217 mg of cerium nitrate precursor was mixed with a 2 mL solution containing 200 mg of citric acid. The resulting mixture was quickly added to 100 mL of 0.4 M ammonium hydroxide. After 24 h of stirring at room temperature, the resulting clear yellow nanoparticle solution was centrifuged at $2600g$ for 30 min to remove aggregates. The supernatant of the centrifuged solution was further purified by centrifugation in 3 kDa molecular weight cutoff tubes. The resulting nanoparticle solution was ultracentrifuged at $15000g$ for 10 min and was subsequently filtered through a 0.02 μm syringe filter. The final nanoparticle solution was suspended in either deionized water or PBS for further studies.

2.3. Nanoparticle Characterization.

The UV/vis absorbance spectra of CeONP were obtained by using a Genesys UV/vis (Thermofisher Scientific) spectrophotometer. The core sizes and morphologies of CeONP were determined by using transmission electron microscopy (TEM). A Tecnai T12 microscope (Field Electron and Ion Co.) was operated at 100 kV to acquire the micrographs. ImageJ software was used to manually measure the diameters of 500 individual nanoparticles for core size analysis. A Nano-ZS Zetasizer system (Malvern Instruments) was used to measure the hydrodynamic diameters and zeta potentials. The concentrations of CeONP solutions were measured by using inductively coupled plasma optical emission spectroscopy (ICP-OES; Spectro Analytical Instruments GmbH). The X-ray diffraction (XRD) pattern of dried CeONP was characterized by a Rigaku GiegerFlex D/Max-B X-ray diffractometer in the range 20°–90° at a scan rate of 2°/min. For energy-dispersive X-ray spectroscopy (EDX), CeONP were dried onto a copper grid before recording their EDX spectra by using a Quanta 600 field emission gun scanning electron microscope. A Physical Electronic VersaProbe 5000 X-ray photo-electron spectrometer

(XPS) was used to study the elemental composition and oxidation states of cerium ions in CeONP. A JASCO FT/IR-480 Plus spectrophotometer was used to collect Fourier transform infrared spectroscopy (FT-IR) spectra of CeONP and citric acid powder.

2.4. *In Vitro* Biocompatibility.

The biocompatibility of CeONP was assessed in HepG2 (hepatocytes), RAW264.7 (macrophages), Renca (epithelial kidney cells), and SVEC4-10EHR1 (endothelial cells) by measuring cell viability after CeONP treatment. Each cell line was seeded at 1×10^5 cells/ well in 24-well plates and was cultured overnight. After the initial cell culture, the media was exchanged with fresh media containing various concentrations of CeONP. The cells were incubated in the CeONP-treated media for 24 h prior to media removal and addition of LIVE/DEAD stain. The cells were stained for 20 min for fluorescent imaging of cell nuclei, live cells, and dead cells at four different fields of view per well. The cell viability was calculated by dividing the live cell count by the total cell count.

2.5. SOD-Mimetic Activity Assay.

The SOD-mimetic activity of CeONP was measured with a SOD colorimetric activity kit (Invitrogen). CeONP stock solution was diluted to varying concentrations in PBS. We added 10 μL of each concentration to wells of a 96-well plate. Upon subsequent additions of the substrate and xanthine oxidase to the wells per instruction, the mixture was incubated at room temperature for 20 min before reading the absorbance at 450 nm.

2.6. Catalase-Mimetic Activity Assay.

The catalase-mimetic activity of CeONP was conducted with an Amplex red hydrogen peroxide/peroxidase assay kit (Molecular Probes, Inc.). CeONP solutions of varying concentrations were prepared in the reaction buffer. After adding 50 μL of CeONP to the wells of a 96-well plate, we subsequently added 50 μL of 40 μM hydrogen peroxide. After 20 min of incubation, 50 μL of working solution was added to each well. The mixture was allowed to react at room temperature for another 30 min before reading the absorbance at 560 nm.

2.7. Intracellular ROS Production Level.

ROS in macrophages were measured by using a ROS sensitive dye, chloromethyl 2′,7′-dichlorodihydrofluorescein diacetate (CM-H$_2$DCFHDA). RAW 264.7 macrophage cells were seeded in 96-well plates at a density of 2×10^4 cells/well and were cultured overnight. Then, the cell culture media was exchanged with fresh media for the lipopolysaccharide (LPS) group and fresh media with 200 ng/mL of LPS for the LPS+ groups to start stimulation. After 1 h, CeONP solutions of different concentrations were added to the cell culture media, and the cells were further incubated for another 24 h. To end LPS stimulation and CeONP treatment, the cells were washed twice with PBS before incubating with 10 μM CM-H$_2$DCFHDA solution for 20 min at 37 °C. At the end of the incubation, the cells were washed and allowed to recover for 5 min at 37 °C. The fluorescence intensity was measured at an excitation wavelength of 492 nm and an emission wavelength of 527 nm. The identical

cell culture and treatment conditions were used to assess hydroxyl radical (·OH) levels by using a HORAC activity assay.

2.8. Cell Protection against Oxidative Damage Induced by Hydrogen Peroxide (H$_2$O$_2$).

The protective effect of CeONP against oxidative damage was studied by incubating cells in H$_2$O$_2$-treated (0.01%) cell culture media in the presence or absence of CeONP. Oxidative damage to BJ5-ta and RAW 264.7 cells was induced by H$_2$O$_2$. In 96-well flat bottom microplates, 2×10^4 cells were seeded to each well and were allowed to acclimate for 24 h. After 24 h, the cells were gently washed with PBS and incubated with either fresh media (control), H$_2$O$_2$-treated media, or CeONP-added, H$_2$O$_2$-treated media for 30 min. H$_2$O$_2$ exposure was stopped after 30 min by replacing the media with fresh cell culture media. Cells were allowed to recover for 4 h, at which point the cell viability was measured by using the MTS assay (CellTiter 96 cell proliferation assay kit from Promega). The cell viability was normalized to the control.

2.9. Pro- and Anti-Inflammatory MRNA Expression and Cytokine Secretion Analysis.

mRNA expression and cytokine release levels of both proinflammatory cytokines (TNFα and IL-1β) and anti-inflammatory cytokine (IL-10) from RAW 264.7 macrophages were assessed. The cells were seeded at a density of 1×10^6 cells/well in 6-well plates and were cultured overnight. At which point, the media were removed and replaced with fresh media with or without LPS to start the LPS stimulation. The LPS and CeONP treatment conditions were identical with the previous setup in the ROS assessment. At the end of the treatment, the media were removed to evaluate the cytokine levels of TNFα, IL-1β, and IL-10 via ELISA kits. The cells were also separately collected to assess mRNA expression levels. RNA isolated from RAW 264.7 macrophages by using Trizol reagent (Thermo Fisher) was subjected to RT-PCR to assess mRNA expression via the following primers: IL-1β-Fwd; 5′-ATGGCAACTGTTCCTG-3′, IL-1β-Rev; 5′-TTAGGAAGACACGGAT-3′, TNFα-Fwd; 5′-ATGAGCACAGAAAGCA-3′, TNFα-Rev; 5′-TCACAGAGCAATGACT-3′, IL-10-Fwd; 5′-ATGCCTGGCTCAGCAC-3′, IL-10-Rev; 5′-TTAGCTTTTCATTTTG-3′, GAPDH-Fwd; 5′-ATGCTGCCCTTACCCCGG-3′, and GAPDHRev; 5′-TTACTCCTTGGAGGCCAT-3′.

2.10. Macrophage Cellular Uptake Assay.

LPS-stimulated, CeONP-treated macrophages were collected and centrifuged at 160 rcf for 5 min. The collected cells were fixed in a 2.5% glutaraldehyde and 2% formaldehyde solution and was cut into thin sections (~60 nm) for TEM analysis.

2.11. Western Blotting Analysis.

Proteins were resolved by SDS-PAGE and transferred onto 0.45 μm PVDF membranes (Millipore). Membranes were blocked overnight at 4 °C with 5% milk in PBS and 0.5% Tween-20 (PBST). Membranes were incubated for 1 h with one of the following antibodies: rat monoclonal anti-CD68 (Abcam; 1:1000), rabbit monoclonal TNFα (Cell Signaling; 1:1000), mouse monoclonal IL-1β (Thermo Fisher; 1:1000), and mouse monoclonal IL-10 (Santa Cruz; 1:1000). This was followed by 1 h incubation with horseradish peroxidase-

coupled goat anti-mouse, anti-rabbit, and anti-rat secondary antibodies (Thermo Fisher; 1:1000). Detections were performed with a Pierce ECL Western blotting substrate (Thermo Fisher). Signals were quantified by using ImageJ.

2.12. *In Vivo* Studies.

All *in vivo* studies were performed on male C57BL/6J mice (Jackson Laboratory) of 12 weeks in age. All procedures were performed in accordance with the guidelines approved by the University of Pennsylvania Institutional Animal Care and Use Committee.

2.12.1. Peripheral Inflammation Model Induction and Paw Edema Thickness.

—Using digital calipers, we measured basal widths of both hind paws of mice immediately before the onset of inflammation. Peripheral inflammation was induced by injecting 20 μL of complete Freund's adjuvant (CFA) in the central plantar region of left hind paws (ipsilateral) subcutaneously.[34] At 24 h post-CFA, the paw thickness of the ipsilateral paw, as index of edema, was measured shortly before the start of treatment (0 h time point). The paw thickness of the contralateral (uninjured) paw was also measured to assess off-target effects of CFA. To assess the *in vivo* immune regulatory effects of CeONP, the mice were randomized to two groups and were administered with either 100 μL of saline (vehicle) or CeONP (dose of 100 mg Ce/kg). Paw thicknesses of both ipsilateral and contralateral paws of each mouse were measured at 3, 6, 18, and 24 h post-treatment in a blinded fashion. The paw thickness at each time point and the net change from the basal width (0 h) were compared between the vehicle injection group and the CeONP treatment group ($n = 8$ per group).

2.12.2. Behavioral Testing: Thermal Pain Hypersensitivity.—The thermal pain

hypersensitivity test was performed by using a heated glass-based plantar analgesiometer (Stoelting). Each mouse was placed in a warmed individual plexiglass cubicle on a glass surface for 1 h daily to allow mice to acclimate to the environment for 3 days. The baseline measurements were taken prior to the CFA injection (–24 h) and prior to the treatment (0 h). An intense focal spot of light beam was created under the paw to produce heat. The paw withdrawal latency (PWL), which was defined as the time between the onset of heat stimulus and paw withdrawal in response, was recorded at 3, 6, 18, and 24 h post-treatment. At each time point, each mouse was tested in five sequential trials with an interval of 2–3 min. The PWL was measured on both ipsilateral and contralateral hind paws.

2.13. *Ex Vivo* Studies.

2.13.1. Biodistribution.—At 24 h post-treatment, mice were sacrificed to analyze the

biodistribution of CeONP. Blood samples, major organs (i.e., heart, lungs, liver, spleen, and kidneys), hind paws, and the remaining carcass from each CeONP-treated mouse were harvested and digested. The concentrations of cerium in the digested samples were measured by using ICP-OES.

2.13.2. Renal Clearance of CeONP.—To further investigate the renal clearance of

CeONP, urine samples of CeONP-treated mice were collected at 3 h postinjection and were placed on copper grids for TEM analysis.

2.13.3. In Vivo Toxicity.—Heart, lungs, liver, spleen, and kidneys from both vehicle and CeONP treatment groups were collected at 24 h post-treatment for histological analysis via H&E staining. Each tissue was sliced at thickness of 12 μm for staining.

2.13.4. In Vivo Immune Response Regulation of CeONP.—Immune regulatory effects of CeONP in acute inflammation were investigated by Western blotting and immunofluorescence of several biomarkers: CD68 (macrophage marker), TNFa and IL-1β (proinflammatory cytokines), and IL-10 (anti-inflammatory cytokine). Histological analysis via H&E staining was also conducted.

2.14. Statistical Analysis.

One-way analysis of variance (ANOVA) and the Tukey–Kramer HSD *post hoc* test were used to examine statistical significance in differences between the groups when there are more than two groups to compare (e.g., *in vitro* experiments and *ex vivo* experiments). The unpaired two-sample *t* test was used when there are only two groups in comparison (e.g., *in vivo* experiments). Data are presented in mean ± SD unless indicated otherwise.

3. RESULTS AND DISCUSSION

3.1. Synthesis and Characterization of Citric Acid-Coated CeONP.

Ultrasmall citric acid-coated CeONP were synthesized via a one-step coprecipitation of cerium precursor and citric acid in ammonium hydroxide as depicted in Figure 1A. CeONP solution had the peak UV–vis absorbance at 265 nm (Figure S1).[9,35] Their citric acid coating provided hydrophilicity and stability for CeONP in physiological buffer solutions, such as PBS (Figure S2). As shown in the transmission electron micrographs (Figure 1B), CeONP are nearly spherical with an average core diameter of 2.8 ± 0.4 nm. Citric acid coating on the surface led to a hydrodynamic diameter that is slightly larger (3.4 ± 1.1 nm) than the core diameter and negative ζ-potential (Figure 1C). EDX verified that the main elemental components of the core nanoparticles are cerium and oxygen (Figure 1D). The XRD diffraction pattern confirmed a fluorite lattice structure of CeONP highlighted by a strong (111) peak (Figure 1E).[36] XPS showed that our CeONP formulation contained 37.1% cerium(III) oxides and 62.9% cerium(IV) oxides (Figure 1F). Similarities in FT-IR spectra of citric acid powder and CeONP demonstrated intact citric acid surface coating (Figure 1G). Notably, the characteristic peak of the C=O vibration at 1701 cm^{-1} from the carboxylic acid group of citric acid was shifted to 1579 cm^{-1} in CeONP, indicating successful binding of citric acid molecules onto the nanoparticle surfaces.[37] The peak at 1396 cm^{-1} from the bending of tertiary hydroxyl group of citric acid was observed in both FTIR spectra.[38]

3.2. *In Vitro* Cytocompatibility of CeONP.

The cytotoxicity of CeONP was examined by assessing the viability of endothelial cells, hepatocytes, kidney epithelial cells, and macrophages upon CeONP treatment via live/dead assay. These cell types were chosen since they will likely have the highest exposure and accumulation from systemic circulation of CeONP *in vivo*. 24 h treatment with 0.1–2.5 mg Ce/mL of CeONP resulted in >97% viability in all four cell types (Figure 2). The lack of substantial reduction in cell viability demonstrates excellent cytocompatibility of

citric acid-coated CeONP. As the cytotoxicity of nanoparticles is largely affected by their physiochemical properties, the biocompatible and stable citrate coating likely prevented induction of toxic effects to these cells. Furthermore, we expect the actual exposure of these cells to CeONP to be much lower in both concentration and time than the parameters used in this experiment due to efficient renal excretion.

3.3. Enzyme-Mimetic Antioxidative Activities.

The main examples of antioxidant enzymes in our body are SOD and catalase, which help break down two predominant forms of cell-derived ROS: superoxide and hydrogen peroxide.[39] SOD-mimetic and catalase-mimetic activities of CeONP were investigated to determine whether the citric acid coating allowed catalysis to occur. A dose-dependent increase in SOD-mimetic activity was observed, demonstrating effective removal of superoxide ions by CeONP (Figure 3A). Similarly, high levels of catalase-mimetic activities of CeONP were also observed in a dose-dependent manner, although the conversion rate ceased to increase at 0.05 mg/mL (Figure 3B). Concentration-dependent increase in ·OH scavenging activity was also shown by CeONP (Figure 3C). These results demonstrate the ability of citric acid-coated CeONP to efficiently catalyze various types of ROS into innocuous molecules.

The recorded catalytic activities are comparable or better when compared to other CeONP formulations that showed efficacy in reducing hepatic ischemia[25] and acute kidney injury.[27]

3.4. *In Vitro* ROS Scavenging Activities.

ROS scavenging activities of CeONP were further demonstrated in a cellular environment by examining intracellular ROS production levels in LPS-stimulated macrophages. LPS stimulation caused a significant elevation in intracellular ROS level ($p < 0.001$), and CeONP treatment resulted in marked suppression (Figure 4A). The reduction was significant even at the lowest treatment concentration of 0.01 mg or 10 μg Ce/mL. This suggests that the presence of low CeONP concentration may be sufficient enough to trigger robust antioxidant effect. ROS scavenging activities of CeONP in macrophages have also been demonstrated by dose-dependent reduction of ·OH levels in the cell culture media (Figure 4B).

TEM analysis of CeONP-treated, LPS-stimulated macrophages revealed active cellular uptake of CeONP at both low (0.05 mg Ce/mL) and high (0.5 mg Ce/mL) treatment concentrations (Figure S3), implying that CeONP can scavenge intracellular ROS by directly interacting with them in macrophages.

It is widely known that macrophages are specialized in elimination of pathogens by producing an excessive amount of reactive species,[4] which subsequently promotes expression of proinflammatory genes, namely TNFα and IL-1β.[5,40,41] Our findings suggest that CeONP can prevent excessive production of ROS in macrophages and therefore can potentially modulate inflammatory responses and alleviate tissue damage from activated macrophages at inflammation sites.

3.5. Protective Effect against Oxidative Damage.

Thirty-minute exposure of BJ-5ta (human fibroblast) and RAW 264.7 cells to H_2O_2 significantly lowered cell viability (Figure 5). When the cells were co-treated with CeONP during the exposure, the decrease in cell viability was much less. Greater cell viabilities in both CeONP-co-treated groups (0.1 and 0.5 mg/mL) versus H_2O_2-treated groups were statistically significant.

3.6. *In Vitro* Anti-Inflammatory Effect.

We assessed both mRNA expression and cytokine secretion of proinflammatory cytokines, TNFα and IL-1β, upon CeONP treatment to validate that ROS scavenging activities of CeONP can lead to suppression of proinflammatory cytokine secretion in macrophages. LPS-induced activation of macrophages elevated mRNA expression of TNFα by more than 6-fold on average and was significantly abated by CeONP treatment at concentrations higher than 0.5 mg/mL (Figure 6A). A similar pattern of dose-dependent inhibition was observed for IL-1β (Figure 6B). Interestingly, significant repression of TNFα and IL-1β secretion was observed at much lower CeONP treatment concentrations (at 0.01 mg/mL for TNFα and 0.1 mg/mL for IL-1β) when compared to those that significantly lowered the mRNA expression (Figure 6D,E). This potentially suggests that CeONP interfere with the release of these cytokines from macrophages rather than their biosynthesis at the time of sample collection (25 h post-LPS stimulation). Dose-dependent reduction of TNFα and IL-1β levels was also observed when the cells were treated with ascorbic acid, a well-established antioxidant (Figure S5), supporting the hypothesis that the inflammatory cytokine suppression from CeONP is largely due to their antioxidant properties. The differences in cytokine production of unstimulated macrophages that were treated and untreated with CeONP were not statistically significant (Figure S6).

We also investigated the effect of CeONP treatment on secretion of IL-10, a potent anti-inflammatory cytokine that is known to inhibit the expression of proinflammatory cytokines.[42] LPS stimulation resulted in a slight increase in mRNA expression of IL-10 (Figure S4A,B). Upon CeONP treatment, the mRNA expression was continuously elevated in a dose-dependent manner. A similar upward trend was observed for cytokine secretion; however, the peak secretion was observed at the concentration of 0.1 mg/mL (Figure S4C). IL-10 secretion levels at 0.5 and 1 mg/mL treatment concentrations were still significantly higher than untreated macrophages.

In addition to its strong antioxidant properties, the differential effects that CeONP have on proinflammatory cytokines (downregulation) and an anti-inflammatory cytokine (upregulation) further highlight their potent anti-inflammatory effects in activated macrophages. It also implies that CeONP can reduce macrophage polarization toward M1-like macrophages and promote polarization toward M2-like macrophages, which can regulate inflammation and promote wound healing by secreting anti-inflammatory cytokine.[43] The peak IL-10 secretion observed at a midrange concentration in our study suggests that there may be an optimal dose of CeONP that can yield the most effective regulation of activated macrophages, which is congruent with previous findings.[25,44]

3.7. *In Vivo* Immune Regulatory Effect in Acute Inflammation.

3.7.1. Paw Edema Reduction.—To evaluate the immune regulatory effect of CeONP *in vivo*, we studied whether CeONP can reduce edema and decrease pain hypersensitivity in a mouse model of acute hind paw inflammation. CFA injection into the left paws of mice induced substantial local inflammation, causing noticeable redness and swelling (Figure S7). A single dose tail vein injection of CeONP 24 h after CFA injection quickly alleviated the edema, as shown by a rapid decline in paw thickness. It demonstrates the efficacy of CeONP in modulation of acute inflammatory response (Figure 7A). Within the CeONP-treated group, significant changes in the paw thickness were observed between 3–18 h postinjection (0.72 ± 0.31 cm, $p < 0.005$) and 6–24 h (0.53 ± 0.22 cm, $p = 0.046$). Vehicle injection, on the other hand, did not cause any significant reduction in paw thickness (0.21 ± 0.41 cm, $p = 0.94$ between 3 and 18 h and 0.26 ± 0.45 cm, $p = 0.99$ between 6 and 24 h). When comparing the changes in paw thickness between CeONP-treated and vehicle-injected groups, we observed a significant difference as early as 6 h postinjection, and the difference continued to grow. No significant changes in contralateral paw thickness and body weight were observed in both groups (Figure S8).

3.7.2. Reduction in Macrophage Recruitment and Proinflammatory Cytokine Expression.—The modulation of acute inflammation in the paw was further examined via histologic analyses and Western blotting. H&E staining of inflamed paws that were injected with the vehicle clearly showed histopathologic alterations and elevated cell density in the region when compared to the sham group (no CFA injection). On the contrary, CeONP treatment led to a significant reduction of both, suggesting attenuation of tissue damage related to inflammatory cell infiltration within 24 h (Figure 7B). Western blot analyses of TNFα, IL-1β, and CD68 also showed elevated levels of all three markers in inflamed paws of vehicle-injected mice in comparison to the sham group. However, paws of CeONP-treated mice showed marked reduction of all three biomarkers at 24 h post-treatment (Figure 7C). Reduction in CD68 implies that the decrease in cell density from H&E staining is partially due to abatement in recruitment and infiltration of macrophage cells to the inflammation site. Western blotting further showed that regulation of acute inflammation in the CeONP-treated group was also influenced by increased IL-10 expression (Figure S9).

Suppression of proinflammatory cytokines and macrophage recruitment as well as upregulation of an anti-inflammatory cytokine were further investigated by immunofluorescence staining. As shown in Figure 8, secretion of both TNFα and IL-1β at the inflammation site was much lower in the CeONP-treated group than the vehicle group. Recruitment of CD68-positive macrophages to the inflamed region was also attenuated in the CeONP treatment group. The yellow areas in the merged images where the cytokines and CD68 markers are colocalized indicate that significant amounts of TNFα and IL-1β were secreted by CD68-positive macrophages when left untreated. IL-10 immunofluorescence analysis also revealed that CeONP treatment led to an upregulation of IL-10 expression at the inflammation site (Figure S10). While a significant portion of IL-10 staining overlapped with CD68-positive macrophages, it was also observed elsewhere in the tissue, indicating IL-10 expression by other immune cells, namely T helper cells and dendritic cells.[45]

Mainly produced by macrophages, TNFα, IL-1β, and other proinflammatory cytokines are key participants in elevating vessel permeability, oxidative stress, and edema formation.[46] As shown in our results, CeONP successfully suppressed the expression of these cytokines from macrophages to rapidly alleviate edema formation. Our results also demonstrate that CeONP reduced recruitment and infiltration of immune cells to the inflammation site. Reduction of CD68-positive macrophages illustrated by both Western blotting and immunofluorescence suggests that a decreased number of circulating monocytes were recruited to the inflammation site and transformed into CD68-positive macrophages.[47] The decrease in monocyte recruitment in CeONP-treated mice is likely caused by the catalytic activities of CeONP, as ROS are known to be main facilitators of circulating monocyte recruitment.[48] Taken together, the ability of CeONP to scavenge free radicals may provide therapeutic benefits by decreasing edema and wound development through moderating proinflammatory cytokine secretion and reducing macrophage recruitment.[49]

3.8. *In Vivo* Analgesic Effect.

CeONP treatment also resulted in significantly reduced pain hypersensitivity, as demonstrated by the improvement in PWL (paw withdrawal latency defined by the time between the onset of heat stimulus and paw withdrawal in response) (Figure 9). A significant difference between the CeONP and vehicle groups was observable as early as 3 h postinjection. PWL of CeONP-treated mice at 3 h postinjection was also significantly higher than PWL at the peak of inflammation (0 h time point), indicating fast-acting analgesic effect of CeONP. By 18 h, the PWL of CeONP-treated mice made a full recovery back to the baseline level before the CFA injection (−24 h time point; p-value = 0.175), further indicating that CeONP can alleviate pain hypersensitivity. On the contrary, the positive correlation between PWL and time after CeONP was not observed in contralateral paw (Figure S11).

The alleviation in pain hypersensitivity could be a result of edema reduction, which can relieve compression of the nervous system at the injury site. It can also be explained by suppression of both ROS and proinflammatory cytokines which are known to be involved in the process of pathological pain.[50]

3.9. Blood Half-Life, Biodistribution, and Renal Clearance.

The blood half-life and biodistribution of CeONP were also investigated in the acute paw inflammation mouse model at 24 h post-treatment to examine CeONP clearance and accumulation of CeONP at the inflamed paw. The blood half-life of CeONP after 100 mg/kg intravenous injection was approximately 29 min (Figure 10A). We found less than 16% ID in the body at 24 h post-treatment, suggesting good clearance from the body (Figure 10B). Efficient excretion of CeONP was confirmed by performing TEM on urine samples that were collected at 3 h postinjection. CeONP were easily found in all of multiple TEM grids that had only a fraction of collected urine (10 μL per grid from ~500 μL of urine sample), suggesting the presence of high CeONP concentration in the sample (Figure 10C).

Small hydrodynamic sizes of CeONP, well under the renal clearance threshold around 5.5 nm, and their favorable surface chemistry likely led to the low average retention of ~16% ID,[32,51] which is comparable to other renally clearable nanoparticles reported to

date.[31,52,53] Most CeONP were retained in liver and spleen. Small amounts of CeONP were also found in the kidney (0.7% ID, 1.6% ID/g), lungs (0.3% ID, 0.7% ID/g), and the remaining carcass (1.2% ID, 0.0% ID/g). A considerable amount of CeONP was also found in the inflamed paw, which was about 7-fold higher than the contralateral paw (Figure 10D). Significantly higher accumulation in the inflamed paw can be explained by increased vascular permeability of the capillaries at the inflammation site.[54]

3.10. *In Vivo* Toxicity.

Rapid and efficient renal clearance of CeONP demonstrated in this study reduces long-term cytotoxicity concerns, since most nanoparticles would be excreted within 24 h of administration and minimize their cellular exposure. Regardless, we examined *in vivo* safety of CeONP via histological analysis of major organs (e.g., heart, lung, liver, spleen, and kidney) as a portion of the injected dose was retained at 24 h postinjection. As shown in Figure 11A, H&E staining of the major organs did not reveal any noticeable signs of acute toxicity or adverse effects in both control (vehicle) and CeONP-treated groups. Comparing the microscopic tissue structures from the two groups of mice, they closely resembled one another without any indication of abnormalities. The differences in the levels of serum biomarkers for liver and kidney functions (i.e., ALT, AST, BUN, and others) between saline- and CeONP-treated mice were not statically significant across all biomarkers analyzed, further demonstrating CeONP's tolerability.

As demonstrated by observation of stable body weight, histological analyses, and serum biomarker levels, we did not observe any severe adverse effects in mice after systemic CeONP administration largely due to both effective clearance and biocompatible surface coating of CeONP. The importance of size, surface chemistry, and coating integrity in nanoparticle toxicity is emphasized as nanoparticle toxicity is heavily dependent on its physiochemical properties.[55] Our findings suggest that citric acid-coated CeONP are biocompatible and highly tolerable even at a high injection dose of 100 mg/kg.

While signs of effective clearance of CeONP have been indicated in this study, more extensive studies on the safety and clearance of our nanoparticles will need to be performed, such as examination at multiple time points for longer durations and in animal models with more comparable physiology to that of humans. Monitoring organ functions via blood biomarkers, especially that of the liver where we observed the highest nanoparticle accumulation, will need to be further examined in a longitudinal study. These studies will improve our understanding of any chronic effects that CeONP may have on different organs and improve the chance of clinical translation.

Dosage is another important parameter to consider in evaluating the safety of CeONP. Previous reports of CeONP formulations with poor particle stability and renal clearance have shown that they can cause organ damage when injected at high doses.[56,57] Although the rapid clearance and stable coating integrity of our CeONP formulation resulted in no noticeable toxicity, optimal dose regimen and administration route can further improve the safety profile of our formulation, while preserving its immune regulatory effects in acute inflammation. It is also expected that potential adverse effects from ROS scavenging

activities in nontarget areas will be minimal as their catalytic activity is limited by the low oxygen concentration inside our body, scavenging ROS only when they are elevated.[44]

The close connection between oxidative stress and inflammation has led to numerous studies that have exploited the immune regulatory effects of nanozymes in treatment of inflammatory diseases.[58,59] While the multiple and reversible reactive sites of CeONP should be advantageous over traditional antioxidants, their comparative therapeutic effects are largely unexplored. Therefore, the relative efficacy of CeONP against inflammatory diseases will be validated in a future head-to-head comparative study of CeONP and traditional antioxidants. The relative efficacy will also be compared to anti-inflammatory drugs (e.g., NSAIDs) for further assessment.

In this study, we demonstrated that CeONP can effectively suppress activation of macrophages, which are the main first line defense against pathogens and the primary contributor for initiation of a cascade of inflammatory processes in acute inflammation.[43,60] Suppression of macrophages was sufficient in modulating acute inflammation in this study. However, inflammation is a complex phenomenon that involves a wide variety of immune cells working in concert. Therefore, understanding the effects of CeONP on cellular functions of other immune cells, such as neutrophils and T cells, would expand their biomedical application to treatment of diseases affected by chronic inflammation (e.g., autoimmune diseases, rheumatoid arthritis, chronic open wounds, and atherosclerosis).

4. CONCLUSIONS

In this study, we synthesized ultrasmall CeONP with strong antioxidant properties that were efficient in ROS scavenging and suppression of inflammatory cytokine secretion in macrophages *in vitro*. This translated to reduction in edema, suppression of macrophage recruitment, and alleviation of pain hypersensitivity *in vivo*. The CeONP nanoparticles were biocompatible and showed rapid excretion from the body to reduce the long-term toxicity concern. Our findings demonstrate that CeONP are promising material for effective modulation of immune response with potential for clinical translation.

Supplementary Material

Refer to Web version on PubMed Central for supplementary material.

ACKNOWLEDGMENTS

REFERENCES

(1). Tan HY; Wang N; Li S; Hong M; Wang X; Feng Y The Reactive Oxygen Species In Macrophage Polarization: Reflecting Its Dual Role in Progression and Treatment of Human Diseases. Oxid. Med. Cell. Longevity 2016, 2016, 2795090.

(2). Rzigalinski BA; Carfagna CS; Ehrich M Cerium Oxide Nanoparticles In Neuroprotection And Considerations For Efficacy And Safety. Wiley Interdiscip. Rev.: Nanomed. Nanobiotechnol 2017, 9 (4), 1–10.

(3). Grulke E; Reed K; Beck M; Huang X; Cormack A; Seal S Nanoceria: Factors Affecting Its Pro-And Anti-oxidant Properties. Environ. Sci.: Nano 2014, 1 (5), 429–444.

(4). Mittal M; Siddiqui MR; Tran K; Reddy SP; Malik AB Reactive Oxygen Species In Inflammation And Tissue Injury. Antioxid. Redox Signaling 2014, 20 (7), 1126–1167.

(5). Hussain T; Tan B; Yin Y; Blachier F; Tossou MC; Rahu N Oxidative Stress And Inflammation: What Polyphenols Can Do For Us? Oxid. Med. Cell. Longevity 2016, 2016, 7432797.

(6). Vaziri ND; Rodriguez-Iturbe B Mechanisms Of Disease: Oxidative Stress And Inflammation In The Pathogenesis Of Hypertension. Nat. Clin. Pract. Nephrol 2006, 2 (10), 582–593. [PubMed: 17003837]

(7). Liang M; Yan X Nanozymes: From New Concepts, Mechanisms, And Standards To Applications. Acc. Chem. Res 2019, 52 (8), 2190–2200. [PubMed: 31276379]

(8). Zhang DY; Liu H; Li C; Younis MR; Lei S; Yang C; Lin J; Li Z; Huang P Ceria Nanozymes With Preferential Renal Uptake For Acute Kidney Injury Alleviation. ACS Appl. Mater. Interfaces 2020, 12 (51), 56830–56838. [PubMed: 33319561]

(9). Naha PC; Hsu JC; Kim J; Shah S; Bouche M; Si-Mohamed S; Rosario-Berrios DN; Douek P; Hajfathalian M; Yasini P; Singh S; Rosen MA; Morgan MA; Cormode DP Dextran-Coated Cerium Oxide Nanoparticles: A Computed Tomography Contrast Agent For Imaging The Gastrointestinal Tract And Inflammatory Bowel Disease. ACS Nano 2020, 14 (8), 10187–10197. [PubMed: 32692538]

(10). Jansman MMT; Liu X; Kempen P; Clergeaud G; Andresen TL; Thulstrup PW; Hosta-Rigau L Hemoglobin-Based Oxygen Carriers Incorporating Nanozymes For The Depletion Of Reactive Oxygen Species. ACS Appl. Mater. Interfaces 2020, 12 (45), 50275–50286. [PubMed: 33124811]

(11). Pinna A; Torki Baghbaderani M; Vigil Hernandez V; Naruphontjirakul P; Li S; McFarlane T; Hachim D; Stevens MM; Porter AE; Jones JR Nanoceria Provides Antioxidant And Osteogenic Properties To Mesoporous Silica Nanoparticles For Osteoporosis Treatment. Acta Biomater. 2021, 122, 365–376. [PubMed: 33359295]

(12). Bao Q; Hu P; Xu Y; Cheng T; Wei C; Pan L; Shi J Simultaneous Blood-Brain Barrier Crossing And Protection For Stroke Treatment Based On Edaravone-Loaded Ceria Nanoparticles. ACS Nano 2018, 12 (7), 6794–6805. [PubMed: 29932327]

(13). Choi SW; Cha BG; Kim J Therapeutic Contact Lens For Scavenging Excessive Reactive Oxygen Species On The Ocular Surface. ACS Nano 2020, 14 (2), 2483–2496. [PubMed: 31935066]

(14). Dutta P; Pal S; Seehra MS; Shi Y; Eyring EM; Ernst RD Concentration Of Ce3+ And Oxygen Vacancies In Cerium Oxide Nanoparticles. Chem. Mater 2006, 18 (21), 5144–5146.

(15). Aneggi E; Boaro M; Leitenburg C d.; Dolcetti, G.; Trovarelli, A. Insights Into The Redox Properties Of Ceria-Based Oxides And Their Implications In Catalysis. J. Alloys Compd 2006, 408–412, 1096–1102.

(16). Korsvik C; Patil S; Seal S; Self WT Superoxide Dismutase Mimetic Properties Exhibited By Vacancy Engineered Ceria Nanoparticles. Chem. Commun 2007, No. 10, 1056–1058.

(17). Izu N; Shin W; Matsubara I; Murayama N Development Of Resistive Oxygen Sensors Based On Cerium Oxide Thick Film. J. Electroceram 2004, 13 (1), 703–706.

(18). Eguchi K; Setoguchi T; Inoue T; Arai H Electrical Properties Of Ceria-Based Oxides And Their Application To Solid Oxide Fuel Cells. Solid State Ionics 1992, 52 (1), 165–172.

(19). Dao NN; Luu MD; Nguyen QK; Kim BS UV Absorption By Cerium Oxide Nanoparticles/Epoxy Composite Thin Films. Adv. Nat. Sci.: Nanosci. Nanotechnol 2011, 2 (4), 045013.

(20). Kwon HJ; Kim D; Seo K; Kim YG; Han SI; Kang T; Soh M; Hyeon T Ceria Nanoparticle Systems For Selective Scavenging Of Mitochondrial, Intracellular, And Extracellular Reactive Oxygen Species In Parkinson's Disease. Angew. Chem., Int. Ed 2018, 57 (30), 9408–9412.

(21). Kwon HJ; Cha MY; Kim D; Kim DK; Soh M; Shin K; Hyeon T; Mook-Jung I Mitochondria-Targeting Ceria Nanoparticles As Antioxidants For Alzheimer's Disease. ACS Nano 2016, 10 (2), 2860–2870. [PubMed: 26844592]

(22). Jeong HG; Cha BG; Kang DW; Kim DY; Yang W; Ki SK; Kim SI; Han J; Kim CK; Kim J; Lee SH Ceria Nanoparticles Fabricated With 6-Aminohexanoic Acid That Overcome Systemic Inflammatory Response Syndrome. Adv. Healthcare Mater 2019, 8 (9), No. e1801548.

(23). Park IS; Mahapatra C; Park JS; Dashnyam K; Kim JW; Ahn JC; Chung PS; Yoon DS; Mandakhbayar N; Singh RK; Lee JH; Leong KW; Kim HW Revascularization And Limb Salvage Following Critical Limb Ischemia By Nanoceria-Induced Ref-1/APE1-Dependent Angiogenesis. Biomaterials 2020, 242, 119919. [PubMed: 32146371]

(24). Kim CK; Kim T; Choi IY; Soh M; Kim D; Kim YJ; Jang H; Yang HS; Kim JY; Park HK; Park SP; Park S; Yu T; Yoon BW; Lee SH; Hyeon T Ceria Nanoparticles That Can Protect Against Ischemic Stroke. Angew. Chem., Int. Ed 2012, 51 (44), 11039–11043.

(25). Ni D; Wei H; Chen W; Bao Q; Rosenkrans ZT; Barnhart TE; Ferreira CA; Wang Y; Yao H; Sun T; Jiang D; Li S; Cao T; Liu Z; Engle JW; Hu P; Lan X; Cai W Ceria Nanoparticles Meet Hepatic Ischemia-Reperfusion Injury: The Perfect Imperfection. Adv. Mater 2019, 31 (40), No. e1902956. [PubMed: 31418951]

(26). Zhang DY; Younis MR; Liu H; Lei S; Wan Y; Qu J; Lin J; Huang P Multi-Enzyme Mimetic Ultrasmall Iridium Nanozymes As Reactive Oxygen/Nitrogen Species Scavengers For Acute Kidney Injury Management. Biomaterials 2021, 271, 120706. [PubMed: 33607543]

(27). Zhang D-Y; Liu H; Younis MR; Lei S; Yang C; Lin J; Qu J; Huang P Ultrasmall Platinum Nanozymes As Broad-Spectrum Antioxidants For Theranostic Application In Acute Kidney Injury. Chem. Eng. J 2021, 409, 127371.

(28). Heckert EG; Karakoti AS; Seal S; Self WT The Role Of Cerium Redox State In The SOD Mimetic Activity Of Nanoceria. Biomaterials 2008, 29 (18), 2705–2709. [PubMed: 18395249]

(29). Karakoti A; Singh S; Dowding JM; Seal S; Self WT Redox-Active Radical Scavenging Nanomaterials. Chem. Soc. Rev 2010, 39 (11), 4422–4432. [PubMed: 20717560]

(30). Celardo I; Pedersen JZ; Traversa E; Ghibelli L Pharmacological Potential Of Cerium Oxide Nanoparticles. Nanoscale 2011, 3 (4), 1411–1420. [PubMed: 21369578]

(31). Hsu JC; Cruz ED; Lau KC; Bouche M; Kim J; Maidment ADA; Cormode DP Renally Excretable And Size-Tunable Silver Sulfide Nanoparticles For Dual-Energy Mammography Or Computed Tomography. Chem. Mater 2019, 31 (19), 7845–7854. [PubMed: 33005070]

(32). Choi HS; Liu W; Misra P; Tanaka E; Zimmer JP; Itty Ipe B; Bawendi MG; Frangioni JV Renal Clearance Of Quantum Dots. Nat. Biotechnol 2007, 25 (10), 1165–1170. [PubMed: 17891134]

(33). Kim J; Silva AB; Hsu JC; Maidment PSN; Shapira N; Noel PB; Cormode DP Radioprotective Garment-Inspired Biodegradable Polymetal Nanoparticles For Enhanced CT Contrast Production. Chem. Mater 2020, 32 (1), 381–391. [PubMed: 33005071]

(34). Chen L; Yang G; Cormode DP; Saigal A; Madhavan S; Mazaleuskaya LL; Grant GR; FitzGerald GA; Grosser T Myeloid Cell mPGES-1 Mediates Inflammatory Pain Hypersensitivity In Mice. bioRxiv 2020, 929422.

(35). Lee SS; Song W; Cho M; Puppala HL; Nguyen P; Zhu H; Segatori L; Colvin VL Antioxidant Properties Of Cerium Oxide Nanocrystals As A Function Of Nanocrystal Diameter And Surface Coating. ACS Nano 2013, 7 (11), 9693–9703. [PubMed: 24079896]

(36). Heckman KL; DeCoteau W; Estevez A; Reed KJ; Costanzo W; Sanford D; Leiter JC; Clauss J; Knapp K; Gomez C; Mullen P; Rathbun E; Prime K; Marini J; Patchefsky J; Patchefsky AS; Hailstone RK; Erlichman JS Custom Cerium Oxide Nanoparticles Protect Against A Free Radical Mediated Autoimmune Degenerative Disease In The Brain. ACS Nano 2013, 7 (12), 10582–10596. [PubMed: 24266731]

(37). Patel U; Chauhan K; Gupte S Synthesis, Characterization And Application Of Lipase-Conjugated Citric Acid-Coated Magnetic Nanoparticles For Ester Synthesis Using Waste Frying Oil. 3 Biotech 2018, 8 (4), 211.

(38). Samavini R; Sandaruwan C; De Silva M; Priyadarshana G; Kottegoda N; Karunaratne V Effect Of Citric Acid Surface Modification On Solubility Of Hydroxyapatite Nanoparticles. J. Agric. Food Chem 2018, 66 (13), 3330–3337. [PubMed: 29565585]

(39). Kanzaki H; Wada S; Narimiya T; Yamaguchi Y; Katsumata Y; Itohiya K; Fukaya S; Miyamoto Y; Nakamura Y Pathways That Regulate ROS Scavenging Enzymes, And Their Role In Defense Against Tissue Destruction In Periodontitis. Front. Physiol 2017, 8, 351. [PubMed: 28611683]

(40). Hsu HY; Wen MH Lipopolysaccharide-Mediated Reactive Oxygen Species And Signal Transduction In The Regulation Of Interleukin-1 Gene Expression. J. Biol. Chem 2002, 277 (25), 22131–22139. [PubMed: 11940570]

(41). Bulua AC; Simon A; Maddipati R; Pelletier M; Park H; Kim K-Y; Sack MN; Kastner DL; Siegel RM Mitochondrial Reactive Oxygen Species Promote Production Of Proinflammatory Cytokines And Are Elevated In TNFR1-Associated Periodic Syndrome (TRAPS). J. Exp. Med 2011, 208 (3), 519–533. [PubMed: 21282379]

(42). Zhang JM; An J Cytokines, Inflammation, And Pain. Int. Anesthesiol. Clin 2007, 45 (2), 27–37. [PubMed: 17426506]

(43). Atri C; Guerfali FZ; Laouini D Role Of Human Macrophage Polarization In Inflammation During Infectious Diseases. Int. J. Mol. Sci 2018, 19 (6), 1801.

(44). Casals E; Zeng M; Parra-Robert M; Fernandez-Varo G; Morales-Ruiz M; Jimenez W; Puntes V; Casals G Cerium Oxide Nanoparticles: Advances In Biodistribution, Toxicity, And Preclinical Exploration. Small 2020, 16 (20), No. e1907322. [PubMed: 32329572]

(45). Iyer SS; Cheng G Role Of Interleukin 10 Transcriptional Regulation In Inflammation And Autoimmune Disease. Crit Rev. Immunol 2012, 32 (1), 23–63. [PubMed: 22428854]

(46). Zelova H; Hosek J TNF-Alpha Signalling And Inflammation: Interactions Between Old Acquaintances. Inflammation Res. 2013, 62 (7), 641–651.

(47). Kang D-W; Kim CK; Jeong H-G; Soh M; Kim T; Choi I-Y; Ki S-K; Kim DY; Yang W; Hyeon T; Lee S-H Biocompatible Custom Ceria Nanoparticles Against Reactive Oxygen Species Resolve Acute Inflammatory Reaction After Intracerebral Hemorrhage. Nano Res. 2017, 10 (8), 2743–2760.

(48). Hackel D; Pflucke D; Neumann A; Viebahn J; Mousa S; Wischmeyer E; Roewer N; Brack A; Rittner HL The Connection Of Monocytes And Reactive Oxygen Species In Pain. PLoS One 2013, 8 (5), No. e63564. [PubMed: 23658840]

(49). Forrester SJ; Kikuchi DS; Hernandes MS; Xu Q; Griendling KK Reactive Oxygen Species In Metabolic And Inflammatory Signaling. Circ. Res 2018, 122 (6), 877–902. [PubMed: 29700084]

(50). Vanderwall AG; Milligan ED Cytokines In Pain: Harnessing Endogenous Anti-Inflammatory Signaling For Improved Pain Management. Front. Immunol 2019, 10, 3009. [PubMed: 31921220]

(51). Liu J; Yu M; Zhou C; Zheng J Renal Clearable Inorganic Nanoparticles: A New Frontier Of Bionanotechnology. Mater. Today 2013, 16 (12), 477–486.

(52). Loynachan CN; Soleimany AP; Dudani JS; Lin Y; Najer A; Bekdemir A; Chen Q; Bhatia SN; Stevens MM Renal Clearable Catalytic Gold Nanoclusters For In Vivo Disease Monitoring. Nat. Nanotechnol 2019, 14 (9), 883–890. [PubMed: 31477801]

(53). Yu M; Xu J; Zheng J Renal Clearable Luminescent Gold Nanoparticles: From The Bench To The Clinic. Angew. Chem., Int. Ed 2019, 58 (13), 4112–4128.

(54). Filewod NC; Lee WL Inflammation Without Vascular Leakage. Science Fiction No Longer? Am. J. Respir. Crit. Care Med 2019, 200 (12), 1472–1476. [PubMed: 31381867]

(55). Sukhanova A; Bozrova S; Sokolov P; Berestovoy M; Karaulov A; Nabiev I Dependence Of Nanoparticle Toxicity On Their Physical And Chemical Properties. Nanoscale Res. Lett 2018, 13 (1), 44. [PubMed: 29417375]

(56). Ma JY; Mercer RR; Barger M; Schwegler-Berry D; Scabilloni J; Ma JK; Castranova V Induction Of Pulmonary Fibrosis By Cerium Oxide Nanoparticles. Toxicol. Appl. Pharmacol 2012, 262 (3), 255–264. [PubMed: 22613087]

(57). Tseng MT; Lu X; Duan X; Hardas SS; Sultana R; Wu P; Unrine JM; Graham U; Butterfield DA; Grulke EA; Yokel RA Alteration Of Hepatic Structure And Oxidative Stress Induced By Intravenous Nanoceria. Toxicol. Appl. Pharmacol 2012, 260 (2), 173–182. [PubMed: 22373796]

(58). Hirst SM; Karakoti AS; Tyler RD; Sriranganathan N; Seal S; Reilly CM Anti-Inflammatory Properties Of Cerium Oxide Nanoparticles. Small 2009, 5 (24), 2848–2856. [PubMed: 19802857]

(59). Selvaraj V; Nepal N; Rogers S; Manne ND; Arvapalli R; Rice KM; Asano S; Fankhanel E; Ma JJ; Shokuhfar T; Maheshwari M; Blough ER Inhibition Of MAP Kinase/NF-kB Mediated Signaling And Attenuation Of Lipopolysaccharide Induced Severe Sepsis By Cerium Oxide Nanoparticles. Biomaterials 2015, 59, 160–171. [PubMed: 25968464]

(60). Hamidzadeh K; Christensen SM; Dalby E; Chandrasekaran P; Mosser DM Macrophages And The Recovery From Acute And Chronic Inflammation. Annu. Rev. Physiol 2017, 79, 567–592. [PubMed: 27959619]
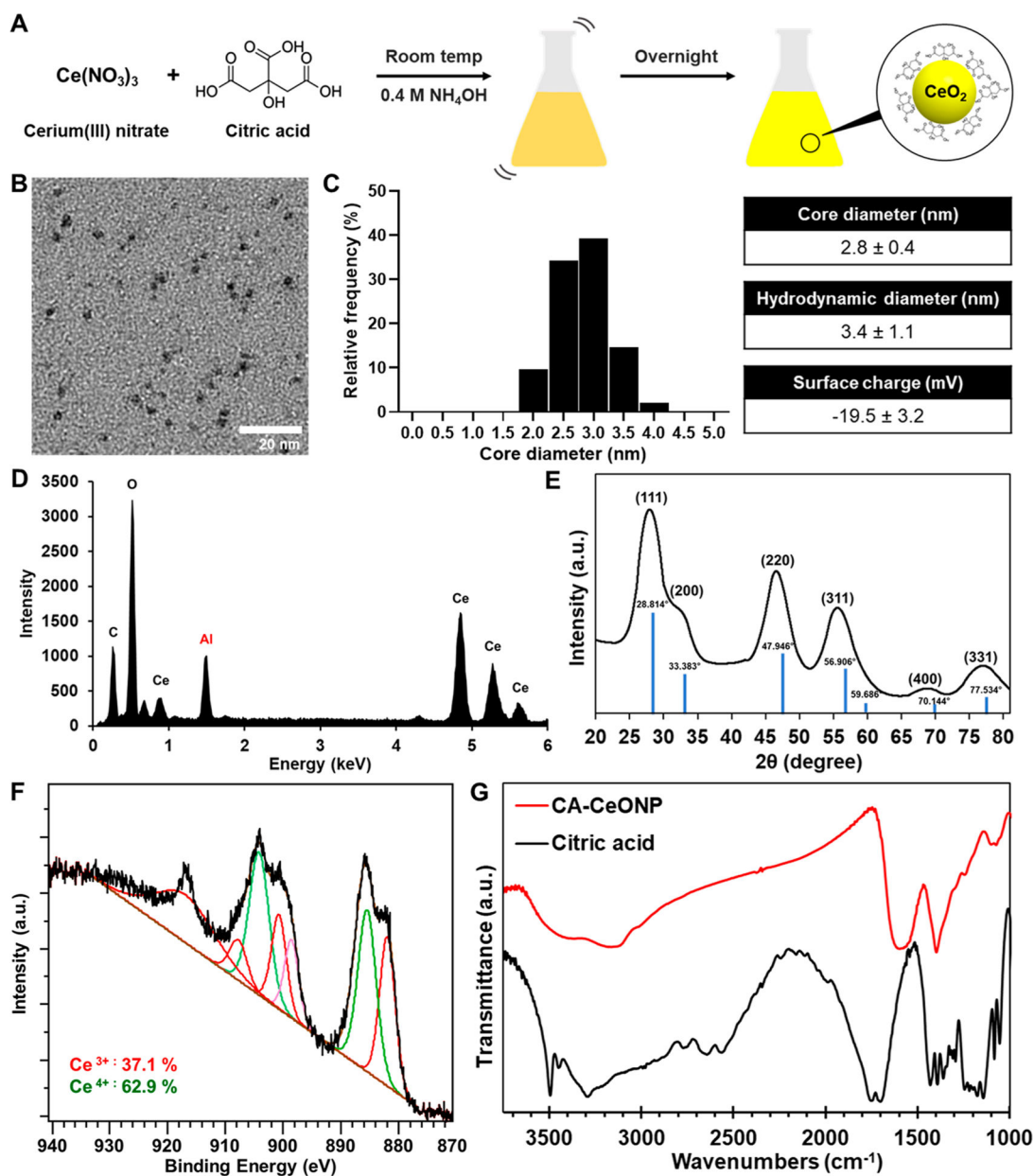
Figure 1.
Characterization of citric acid-coated CeONP. (A) Schematic depiction of CeONP synthesis. (B) Micrograph from TEM, (C) core and hydrodynamic diameters and surface charge, (D) EDX spectrum, (E) XRD pattern (including cerium(IV) oxide peaks as the reference), (F) XPS analysis of CeONP. (G) FTIR spectra of citric acid and CeONP.
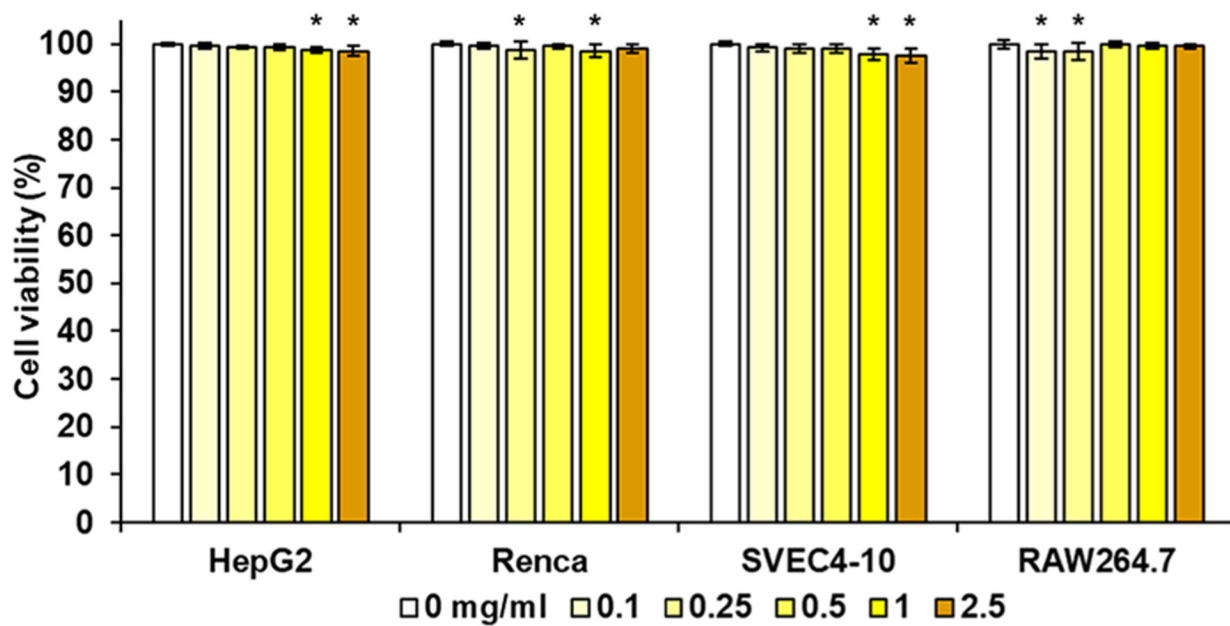
Figure 2.
In vitro biocompatibility of CeONP. Cell viability of HepG2, Renca, SVEC4-10, and RAW264.7 after 24 h of CeONP treatment normalized to no treatment group (mean ± SD; $n = 12$; $*p < 0.05$).
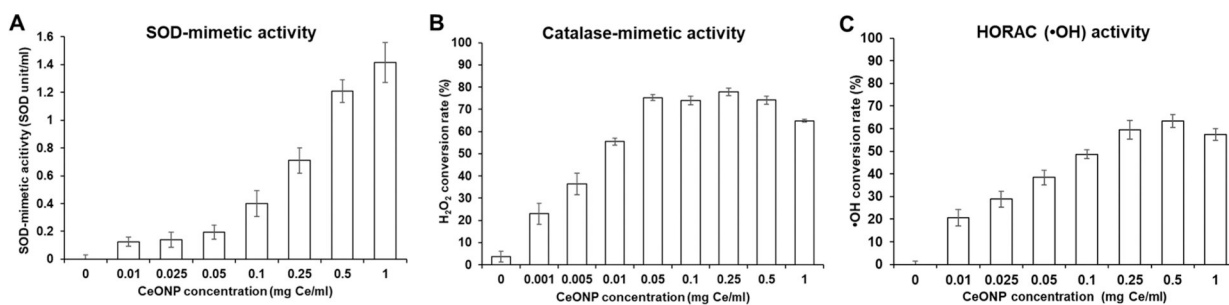
Figure 3.
ROS scavenging activities of CeONP. Scavenging efficiency of CeONP against (A) superoxide ion, (B) hydrogen peroxide, and (C) hydroxyl radical (mean ± SD; $n = 9$).
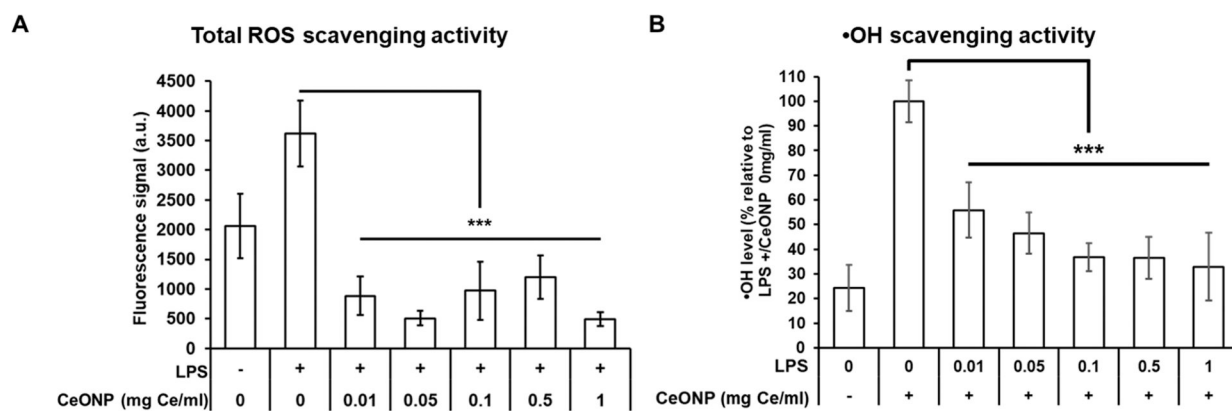
Figure 4.
ROS scavenging activity of CeONP. (A) Intracellular ROS production and (B) ·OH levels of unstimulated and LPS-stimulated macrophages upon CeONP treatment (mean ± SD; $n = 9$; ***$p < 0.001$).
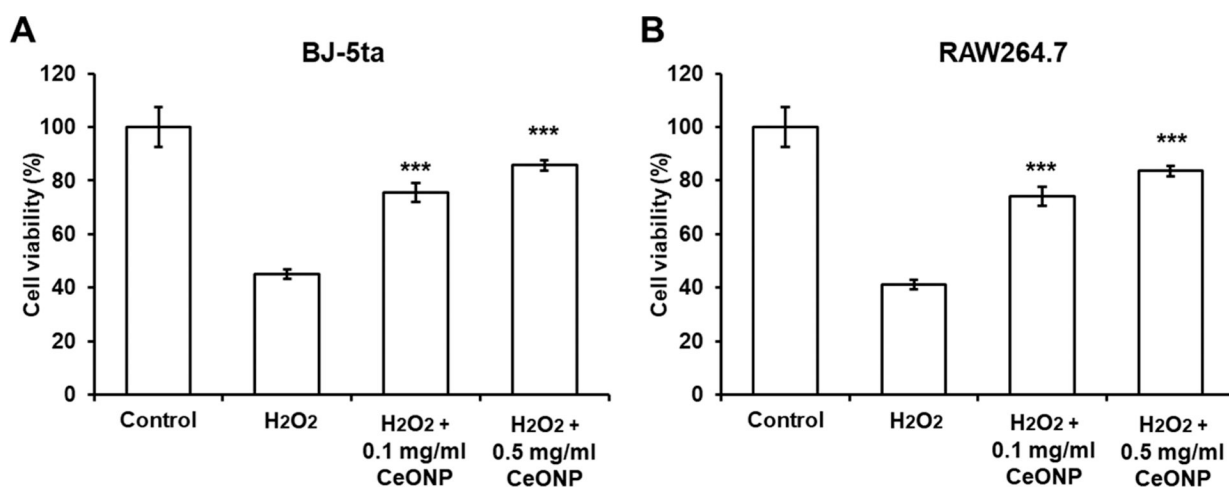
Figure 5.
Protective effect of CeONP against H_2O_2-induced oxidative damage in (A) BJ-5ta and (B) RAW264.7 cells. CeONP-co-treated groups were compared to the H_2O_2-treated groups for statistical tests (data presented as mean ± SD; $n = 8$; ***$p < 0.001$).
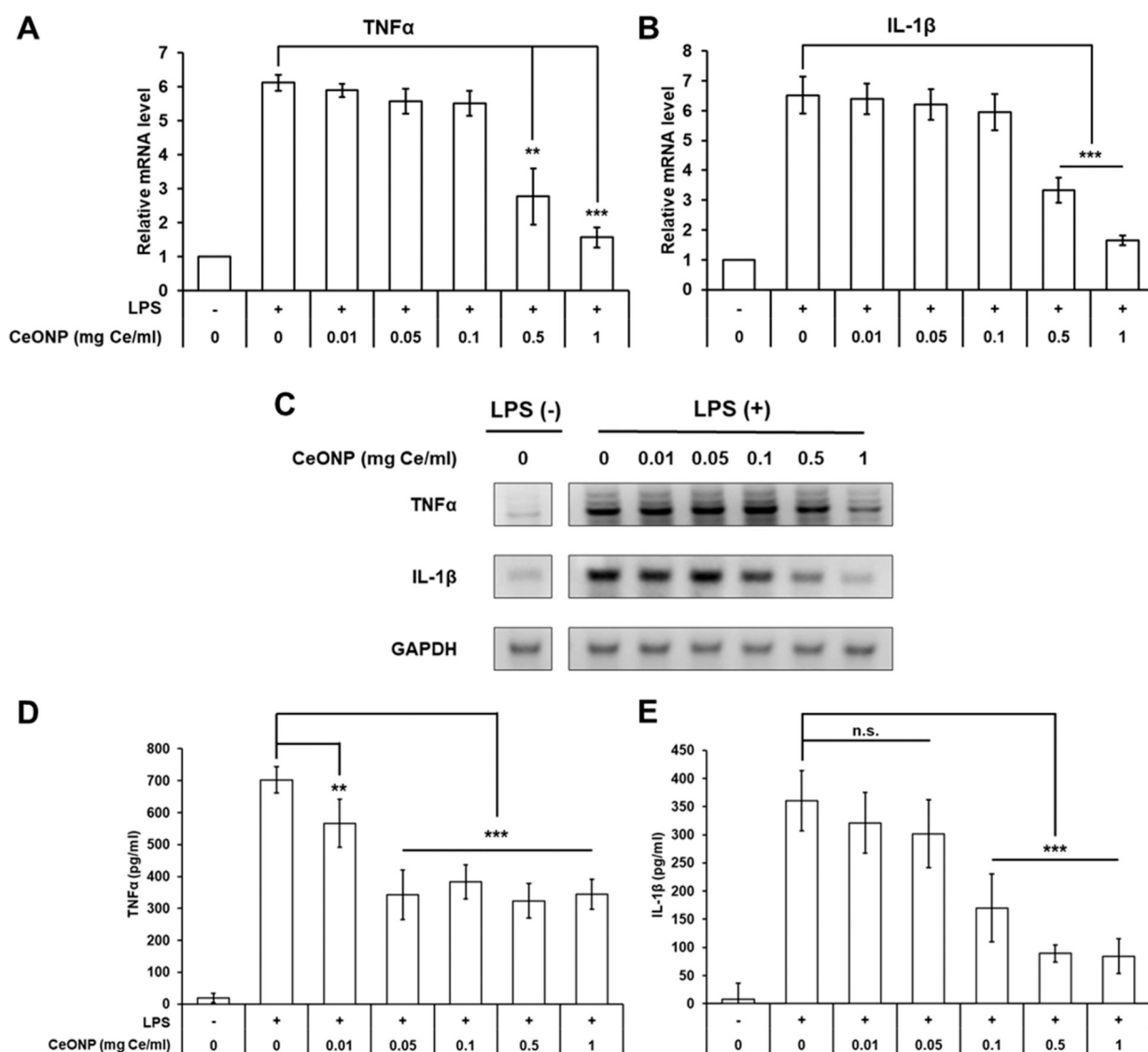
Figure 6.
In vitro anti-inflammatory effect of CeONP in LPS-stimulated macrophage cells. mRNA expression levels of (A) TNFα, (B) IL-1β, and (C) representative mRNA gel electrophoresis image normalized to GAPDH. Cytokine secretion of (D) TNFα and (E) IL-1β (mean ± SD; $n = 9$ for mRNA, $n = 6$ for cytokine; n.s. not significant, **$p < 0.01$, ***$p < 0.001$ relative to untreated, LPS-stimulated group).
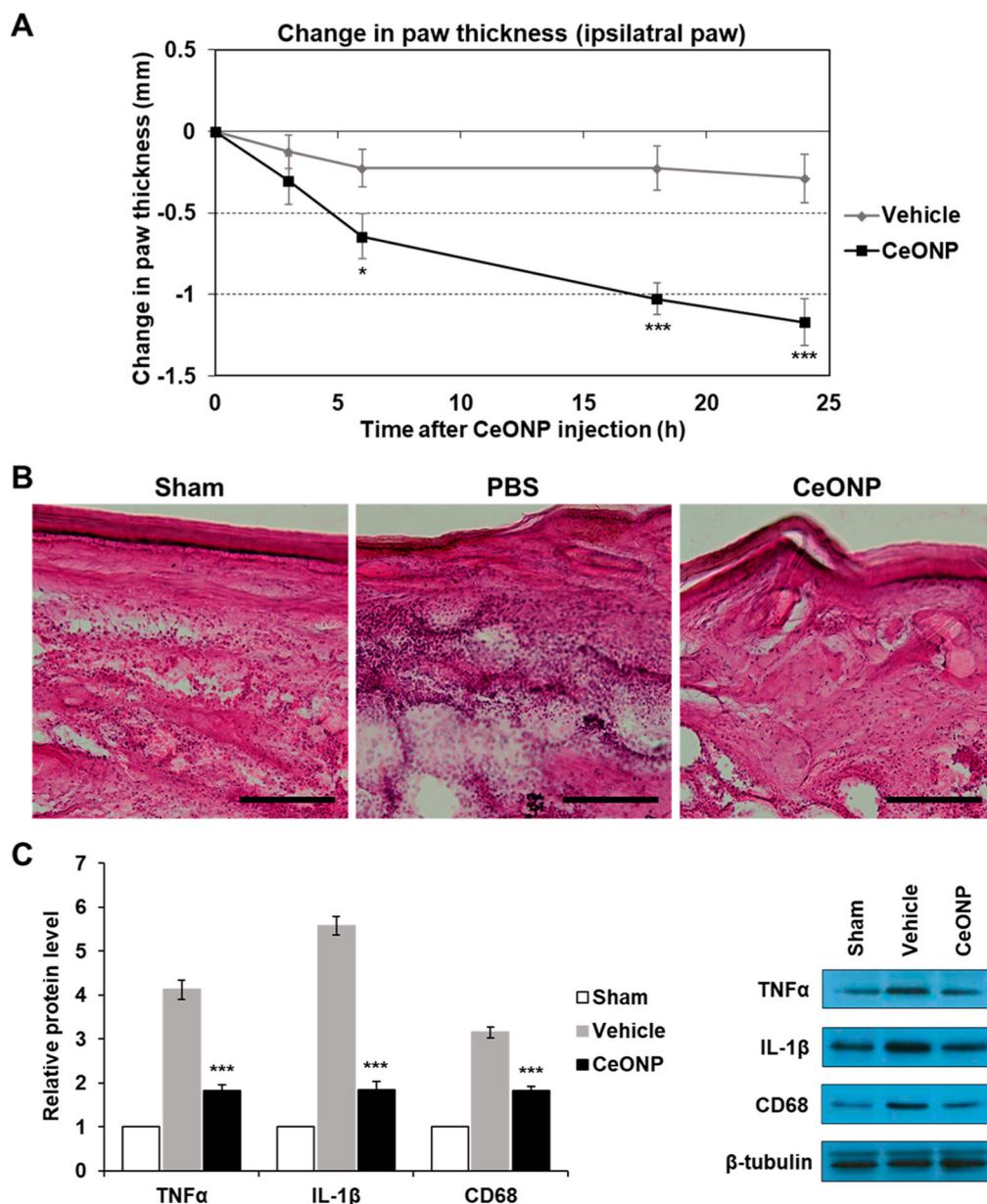
Figure 7.
In vivo edema reduction, suppression of proinflammatory cytokines, and macrophage recruitment in acute hind paw inflammation. (A) Change in paw thickness over 24 h post-CeONP treatment compared to the peak of inflammation induced by CFA (0 h). (B) H&E staining of acute inflammation site from sham (no CFA-induced inflammation), vehicle, and CeONP treatment groups. Scale bar = 50 μm. (C) Western blot analysis of TNFa, IL-1β, and CD68 in inflamed paws of each group (mean ± SEM; $n = 8$ for paw thickness, $n = 4$ for Western blot; * $p < 0.05$, **$p < 0.01$, and ***$p < 0.001$ relative to the vehicle group in (A) and the sham group in (C)).
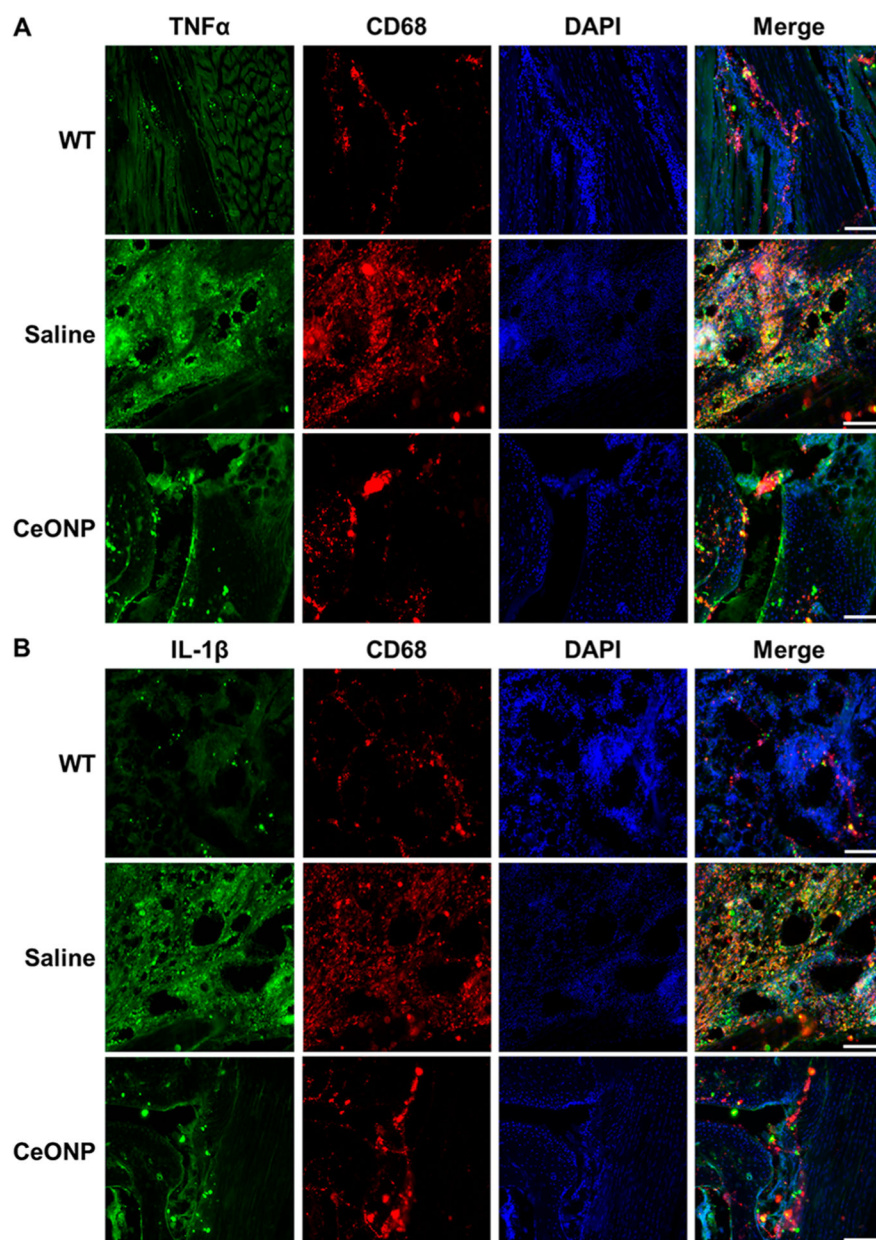
Figure 8.
Immunofluorescence analysis of proinflammatory cytokines and a macrophage marker.
(A) TNFα and (B) IL-1β colocalized with CD68. Scale bar = 200 μm (representative micrographs of three replicates).
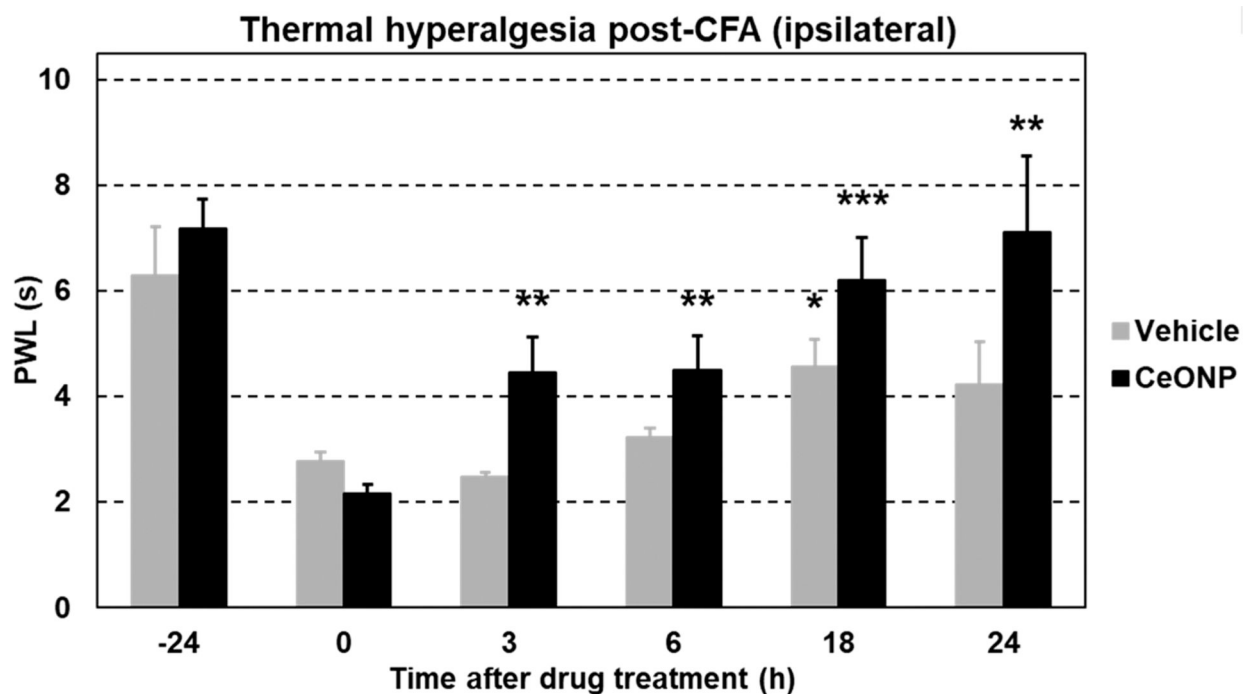
Figure 9.

Thermal pain hypersensitivity in the hind paw acute inflammation model. PWL of mice injected with the vehicle and CeONP over 24 h postinjection (mean ± SEM; $n = 4$ per group; $*p < 0.05$, $**p < 0.01$, and $***p < 0.001$ relative to PWL at 0 h time point in the respective groups).
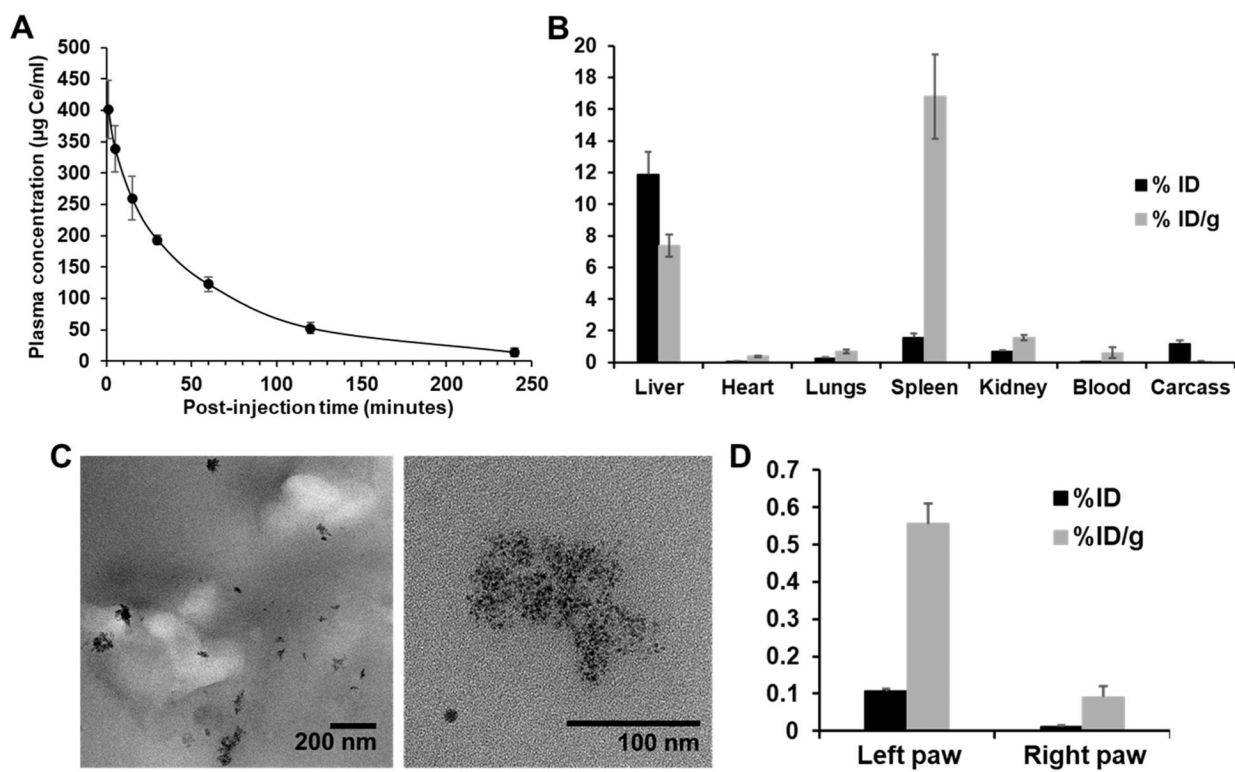
Figure 10.

In vivo blood clearance and biodistribution of CeONP in a CFA model of hind paw inflammation. (A) Blood clearance of CeONP. (B) Accumulation of CeONP in the major organs and the remaining carcass. (C) TEM of urine samples from CeONP-treated mice collected at 3 h postinjection. (D) Accumulation of CeONP in the ipsilateral and contralateral paws of mice at 24 h postinjection as measured by ICP-OES (mean ± SD; *n* = 8; *$p < 0.05$, **$p < 0.01$, and ***$p < 0.001$ relative to PWL at 0 h time point in the respective groups).
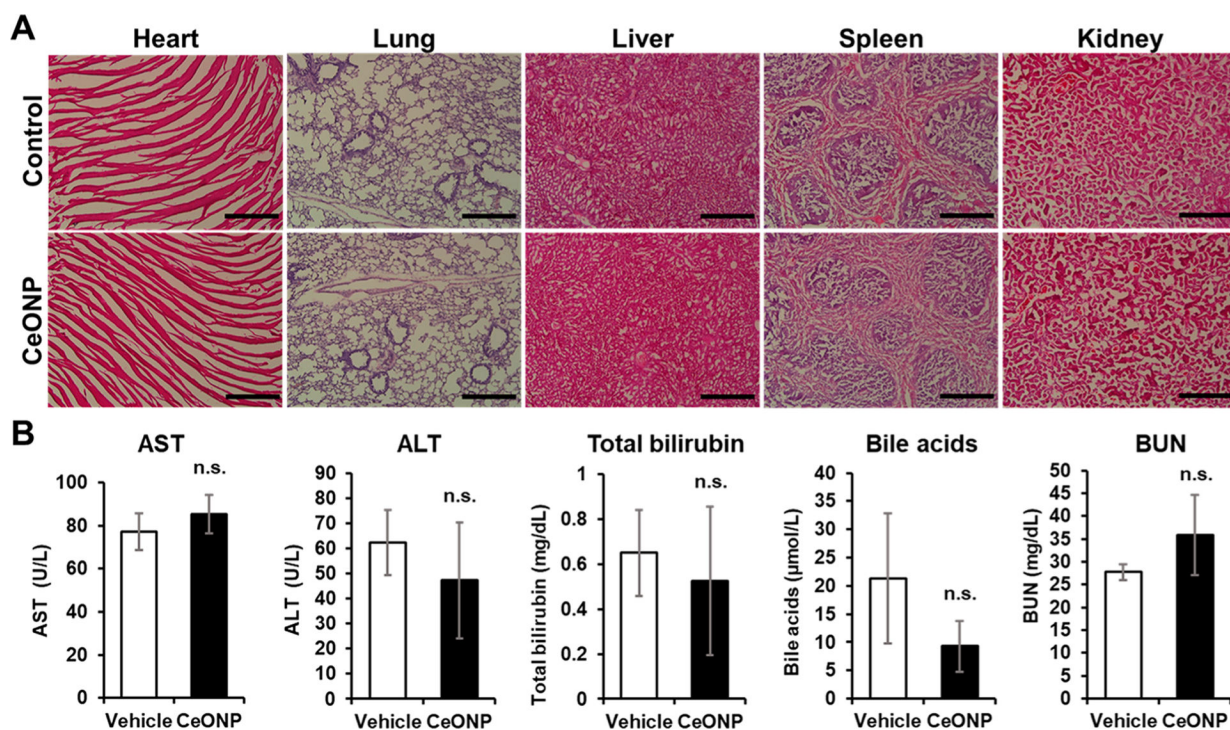
Figure 11.
In vivo toxicity of CeONP from histological and biomarker analysis. (A) Micrographs of H&E-stained major organs (heart, lung, liver, spleen, and kidney) and (B) serum biomarker levels of liver and kidney functions from mice 24 h after injection with the vehicle (control) or CeONP at 100 mg kg^{-1}. Scale bar = 50 μm (mean ± SEM; n = 4 per group; n.s. = not significant relative to the vehicle).